Article

Cell Reports

PARN and TOE1 Constitute a 3′ End Maturation Module for Nuclear Non-coding RNAs

Graphical Abstract

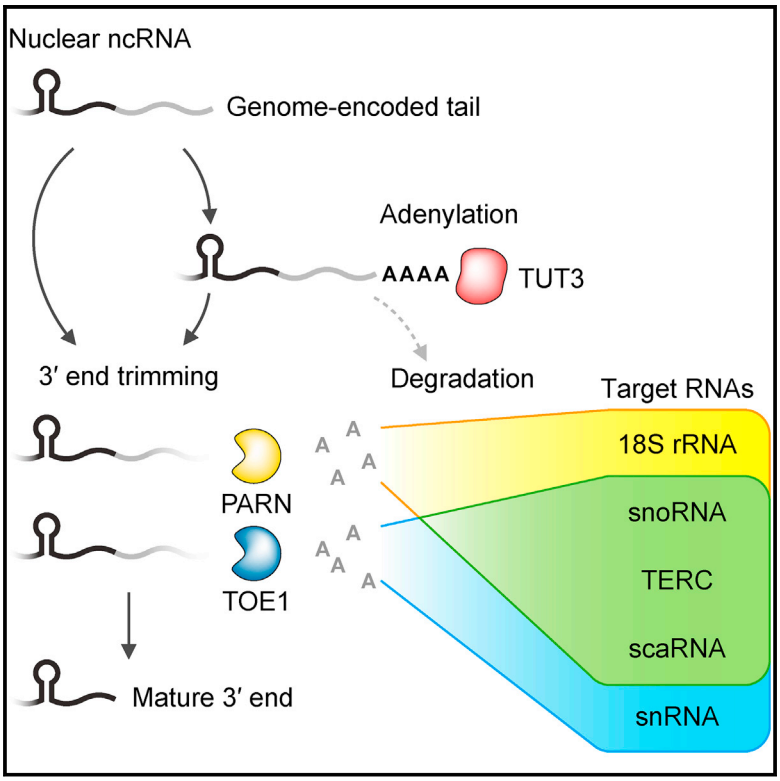

Authors

Ahyeon Son, Jong-Eun Park, V. Narry Kim

Correspondence

narrykim@snu.ac.kr

In Brief

By analyzing the 3′ termini of transcriptome, Son et al. reveal the targets of PARN and TOE1, two nuclear deadenylases with disease associations. Both deadenylases are involved in nuclear small non-coding RNA maturation, but not in mRNA deadenylation. Their combined activity is particularly important for biogenesis of scaRNAs and TERC.

Highlights

- The RNA targetome of PARN and TOE1 is explored on a genomic scale
- PARN and TOE1 are not involved in mRNA deadenylation
- Short nuclear non-coding RNAs, particularly scaRNAs and TERC, are their main targets
- PARN and TOE1 shield immature RNAs from decay and trim their 3′ tails for maturation

Data and Software Availability

GSE111511

Son et al., 2018, Cell Reports *23*, 888–898
April 17, 2018 © 2018 The Author(s).
https://doi.org/10.1016/j.celrep.2018.03.089

CellPress

OPEN ACCESS
CellPress

Cell Reports
Article

PARN and TOE1 Constitute a 3′ End Maturation Module for Nuclear Non-coding RNAs

Ahyeon Son,[1,2,4] Jong-Eun Park,[1,2,3,4] and V. Narry Kim[1,2,5,*]
[1]Center for RNA Research, Institute for Basic Science, Seoul 08826, Korea
[2]School of Biological Sciences, Seoul National University, Seoul 08826, Korea
[3]Wellcome Trust Sanger Institute, Hinxton, Cambridge CB10 1SA, UK
[4]These authors contributed equally
[5]Lead Contact
*Correspondence: narrykim@snu.ac.kr
https://doi.org/10.1016/j.celrep.2018.03.089

SUMMARY

Poly(A)-specific ribonuclease (PARN) and target of EGR1 protein 1 (TOE1) are nuclear granule-associated deadenylases, whose mutations are linked to multiple human diseases. Here, we applied mTAIL-seq and RNA sequencing (RNA-seq) to systematically identify the substrates of PARN and TOE1 and elucidate their molecular functions. We found that PARN and TOE1 do not modulate the length of mRNA poly(A) tails. Rather, they promote the maturation of nuclear small non-coding RNAs (ncRNAs). PARN and TOE1 act redundantly on some ncRNAs, most prominently small Cajal body-specific RNAs (scaRNAs). scaRNAs are strongly downregulated when PARN and TOE1 are compromised together, leading to defects in small nuclear RNA (snRNA) pseudouridylation. They also function redundantly in the biogenesis of telomerase RNA component (TERC), which shares sequence motifs found in H/ACA box scaRNAs. Our findings extend the knowledge of nuclear ncRNA biogenesis, and they provide insights into the pathology of PARN/TOE1-associated genetic disorders whose therapeutic treatments are currently unavailable.

INTRODUCTION

Adenylation and deadenylation provide a deeply conserved regulatory module with diverse functions. In bacteria, adenylation marks mRNAs to trigger degradation, whereas eukaryotic mRNAs utilize polyadenylation for enhanced stability and translation (Dreyfus and Régnier, 2002). Adenylation and deadenylation also serve to degrade aberrant transcripts or to process non-coding RNAs (ncRNAs) (Houseley et al., 2006). Unlike bacterial exonucleases that degrade both adenosine tail and other polynucleotides in the RNA body (Dreyfus and Régnier, 2002), a group of eukaryotic 3′–5′ exonucleases favor adenosine over the other nucleosides (Garneau et al., 2007). These deadenylases are classified into two superfamilies, i.e., DEDD (Asp-Glu-Asp-Asp) or exonuclease-endonuclease-phosphatase (EEP), based on the catalytic domain structure (Goldstrohm and Wickens, 2008). Vertebrates have more than ten deadenylases with distinct subcellular localization and binding partners, suggesting specialized target specificities or modes of regulation in RNA metabolic pathways.

Poly(A)-specific ribonuclease (PARN) has been suspected as a key regulator of mRNAs as it has a preference for 7-methylguanosine (m^7G) cap (Virtanen et al., 2013). Since PARN was shown to cause global poly(A) shortening during *Xenopus* oocyte maturation (Copeland and Wormington, 2001; Kim and Richter, 2006; Körner et al., 1998), evidence supporting the role of PARN in mRNA metabolism has emerged (Cevher et al., 2010; Devany et al., 2013; Gherzi et al., 2004; Lai et al., 2003; Lee et al., 2012; Lejeune et al., 2003; Lin et al., 2007; Miller and Gomez-Cambronero, 2017; Moraes et al., 2006; Reinhardt et al., 2010; Udagawa et al., 2012; Zhang and Yan, 2015; Zhang et al., 2015; Zhu et al., 2011). However, conflicting results were obtained in a study of deadenylation kinetics, suggesting that PARN may not be a vital enzyme in cytoplasmic mRNA deadenylation (Yamashita et al., 2005).

PARN also functions to promote the maturation of ncRNAs, which include small nucleolar RNAs (snoRNAs); small Cajal body-specific RNAs (scaRNAs); and telomerase RNA component (TERC), Y RNAs, and microRNA-451 (Berndt et al., 2012; Boyraz et al., 2016; Dhanraj et al., 2015; Moon et al., 2015; Nguyen et al., 2015; Shukla and Parker, 2017; Shukla et al., 2016; Tseng et al., 2015; Yoda et al., 2013). The precursors of these RNAs have 3′ extensions that are trimmed by exonucleases (Kiss et al., 2006; Matera et al., 2007; Schmidt and Cech, 2015). In the middle of the trimming process, an adenosine tail is often added to processing intermediates, and PARN targets the oligo(A) tail not only to remove it but also to finalize the 3′ end formation (Berndt et al., 2012; Boyraz et al., 2016; Moon et al., 2015; Nguyen et al., 2015; Shukla et al., 2016; Tseng et al., 2015). This exonucleolytic activity of PARN is required for the stable expression of TERC, and a deficiency in PARN causes telomere-related congenital disorders, such as bone marrow failure and pulmonary fibrosis (Boyraz et al., 2016; Burris et al., 2016; Dhanraj et al., 2015; Kropski et al., 2017; Petrovski et al., 2017; Stuart et al., 2015; Tummala et al., 2015).

A more recent report showed that another deadenylase, target of EGR1 protein 1 (TOE1, also known as CAF1Z), participates in small nuclear RNA (snRNA) biogenesis (Lardelli et al., 2017). Biallelic *TOE1* mutations are associated with a neurodegenerative syndrome called pontocerebellar hypoplasia type 7, and cells

This is an open access article under the CC BY license (http://creativecommons.org/licenses/by/4.0/).

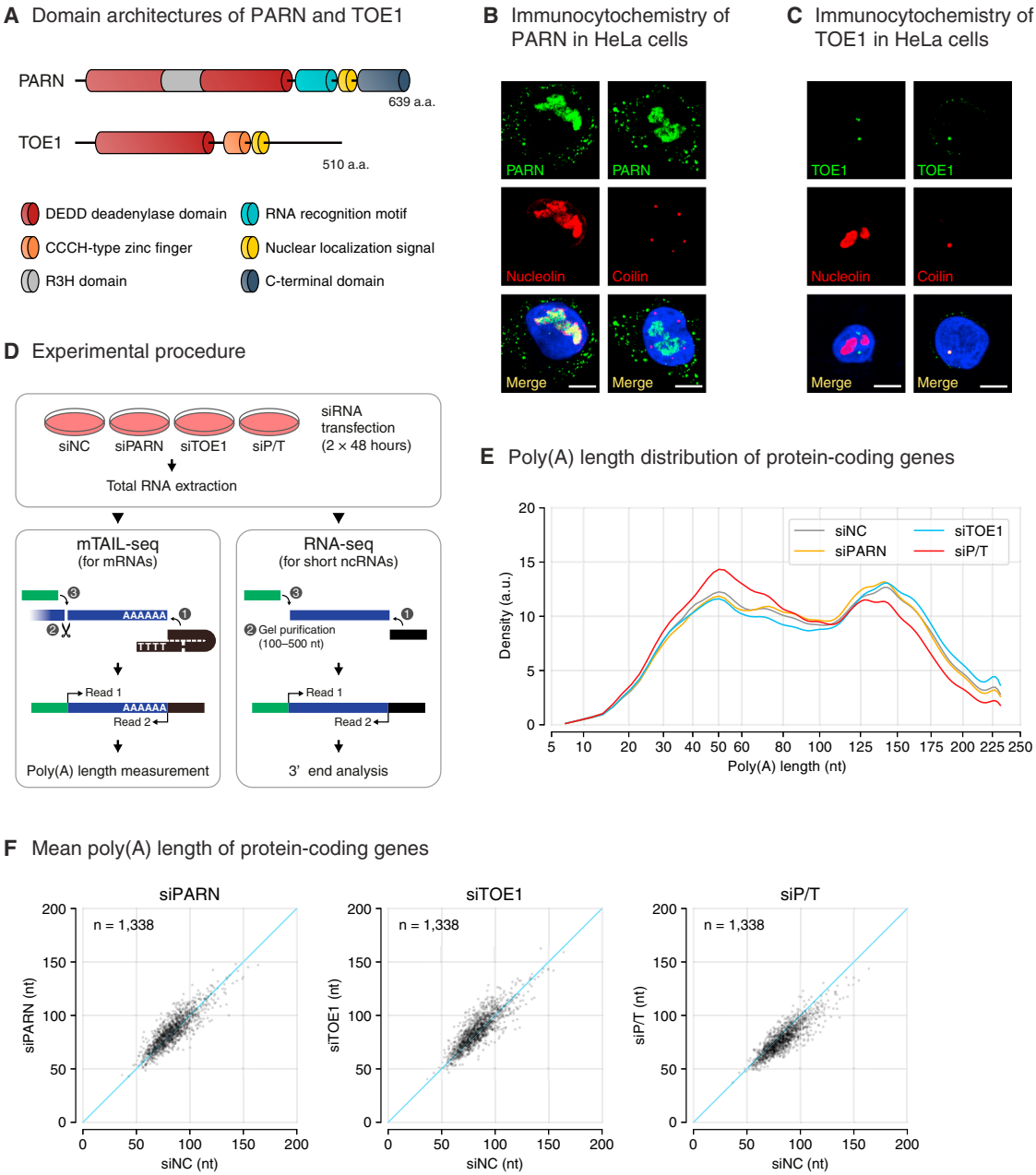

Figure 1. PARN and TOE1 Localize to Nucleolus and Cajal Bodies, Respectively, and They Do Not Act on mRNA Poly(A) Tails

(A) Domain structures of PARN and TOE1.

(B) Immunofluorescence of PARN in HeLa cells. Nucleolin and Coilin were used to show the locations of the nucleolus and Cajal bodies, respectively. Scale bar represents 10 μm.

(C) Immunofluorescence of TOE1 in HeLa cells as in (B). Scale bar represents 10 μm.

(D) Schematic description of the experimental procedure. Samples obtained from PARN/TOE1-depleted HeLa cells are referred to as siP/T. See the Experimental Procedures for details.

(E) Global distribution of poly(A) tail lengths (7–232 nt). The median poly(A) tail lengths are 90 nt in siNC, 92 nt in siPARN, 95 nt in siTOE1, and 79 nt in siP/T.

(F) Mean poly(A) tail lengths of protein-coding genes. The median mean poly(A) lengths are 82 nt in siNC, 84 nt in siPARN, 85 nt in siTOE1, and 77 nt in siP/T. See also Figure S1 and Table S1.

derived from the patients displayed the accumulation of immature snRNAs (Lardelli et al., 2017). Similar to PARN, TOE1 belongs to the DEDD superfamily and contains a nuclear localization signal (Figure 1A). PARN and TOE1 are the only deadenylases with nuclear body localization (Goldstrohm and Wickens, 2008); PARN is mainly detected in the nucleolus and TOE1 is

located in the Cajal bodies (Berndt et al., 2012; Fong et al., 2013). These nuclear bodies are the sites of ncRNA maturation and ribonucleoprotein particle (RNP) assembly (Mao et al., 2011). Furthermore, both PARN and TOE1 were reported to shuttle between the nucleus and cytoplasm and erode mRNAs (Wagner et al., 2007; Yamashita et al., 2005).

Considering the significance of PARN and TOE1 in multiple human diseases, understanding their targetome is important for the development of therapeutic approaches. Most of the functional studies on PARN or TOE1 have relied on *in vitro* or *in vivo* reporter assays (Cevher et al., 2010; Copeland and Wormington, 2001; Gherzi et al., 2004; Kim and Richter, 2006; Körner et al., 1998; Lai et al., 2003; Lejeune et al., 2003; Lin et al., 2007; Miller and Gomez-Cambronero, 2017; Moraes et al., 2006; Wagner et al., 2007; Yamashita et al., 2005; Zhang et al., 2015). Some recent studies have employed deep sequencing (Berndt et al., 2012; Boyraz et al., 2016; Lardelli et al., 2017; Moon et al., 2015; Nguyen et al., 2015; Shukla and Parker, 2017; Shukla et al., 2016; Tseng et al., 2015), but these analyses were restricted to specific RNA species. These methods did not provide a comprehensive perspective on the activity of these enzymes. Moreover, the target specificities of PARN and TOE1 have not been compared yet despite the similarities between them.

In this study, we obtained the RNA targetome of PARN and TOE1 by surveying the tails of mRNAs and short nuclear ncRNAs. Our transcriptomic approach revealed that nuclear RNAs, but not mRNAs, are prime targets of these two deadenylases. We discovered that PARN and TOE1 show both unique and overlapping specificities. The precursors of 18S rRNA and snRNAs are exclusive substrates of PARN and TOE1, respectively. PARN and TOE1 can act redundantly on several RNA classes, which include scaRNAs and TERC, and their combined activity is critical for maintaining the functionality of scaRNPs and telomerase.

RESULTS

PARN and TOE1 Do Not Act on mRNA Tails

To dissect PARN and TOE1 functionally, we first investigated the subcellular localization of these enzymes in our HeLa cell line (Figures 1B, 1C, and S1A). PARN was predominantly found in the nucleolus and cytoplasmic foci (Figure 1B). TOE1 was co-localized with Coilin, the marker protein of Cajal body (Figure 1C). These observations are consistent with previous reports (Berndt et al., 2012; Fong et al., 2013), showing that the HeLa cell is a relevant system to study both proteins. Of note, we could not detect co-localization of PARN with Cajal bodies. This implies that PARN and TOE1 do not share their territories despite the similar domain structure and subnuclear localization.

Next, we examined their activities on two groups of putative RNA targets by applying two high-throughput sequencing methods after the knockdown of either PARN or TOE1 in HeLa cells (Figures 1D and S1B). First, to analyze poly(A) tails of translatable transcripts, we performed mTAIL-seq. Briefly, adenylated RNAs were ligated to and purified by using biotinylated hairpin adapter (Lim et al., 2016). After paired-end sequencing, a machine learning algorithm was used to determine the poly(A) tail length of each RNA species, as described in our previous reports (Chang, 2017; Chang et al., 2014). Despite many reports showing roles in mRNA regulation (Cevher et al., 2010; Devany et al., 2013; Gherzi et al., 2004; Kim and Richter, 2006; Lai et al., 2003; Lee et al., 2012; Lejeune et al., 2003; Lin et al., 2007; Miller and Gomez-Cambronero, 2017; Moraes et al., 2006; Reinhardt et al., 2010; Udagawa et al., 2012; Zhang and Yan, 2015; Zhang et al., 2015; Zhu et al., 2011), the depletion of PARN or TOE1 failed to reshape the poly(A) tail length distribution (Figure 1E). Moreover, none of the individual genes showed significant changes in their poly(A) tail length (Figures 1F and S1C). When PARN and TOE1 were depleted together, poly(A) tails were moderately shortened (Figures 1E, 1F, and S1C). To validate the mTAIL-seq data, we also carried out bulk poly(A) tail assay using two different sets of small interfering RNAs (siRNAs) (Figure S1D). Consistent with mTAIL-seq data, the overall poly(A) tail profile was unaffected after knockdown of either PARN or TOE1. We could not detect any substantial changes even upon double knockdown. Hence, the modest shortening of poly(A) tails in the mTAIL-seq analysis might be due to technical variability. Lastly, mRNA abundance estimated from mTAIL-seq reads remained largely unchanged (Figure S1E), suggesting that neither PARN nor TOE1 affects mRNA turnover. Based on these findings, we concluded that mRNAs are not the major targets of PARN and TOE1.

PARN and TOE1 Determine the 3′ Termini of Nuclear Small ncRNAs

To explore the 3′ terminome of smaller RNAs (<500 nt), rRNA-depleted RNAs were subjected to 3′ adapter ligation and subsequent size fractionation (100–500 nt) without any fragmentation step (Figure 1D). Consequently, 40.3% of sequencing reads were mapped to short nuclear ncRNAs (snRNAs, snoRNAs, and scaRNAs) (Figure S2A). In addition, >50% of the alignments had the exact 3′ ends of known annotations (Figure 2A), indicating the successful enrichment of short nuclear ncRNAs.

By preserving intact 3′ ends, our methodology enabled the 3′ end mapping at a single-nucleotide resolution and the detection of untemplated RNA tails. Short nuclear ncRNAs often had 3′ terminal modifications, among which adenylation was the most frequent one, regardless of RNA classes (Figure S2B). In the control siRNA-transfected cells, approximately 1% of short nuclear ncRNAs were adenylated, and most of them carried a single adenosine tail at their 3′ ends (Figures 2B and S2C). When either PARN or TOE1 was knocked down alone, the fraction of adenylated transcripts was roughly doubled and they had longer tails (Figures 2B and S2C). The elevated frequency of adenylation was more evident for premature RNAs, which contained a 3′ genome-encoded tail of up to 15 nt (Figure 2C). These data suggest that PARN and TOE1 act on precursors of short nuclear ncRNAs and that their action may be the determinant for 3′ end formation. Above all, the adenylation frequency increased upon the co-depletion of PARN and TOE1 (Figures 2B and 2C). Thus, our results show that PARN and TOE1 indeed act on short nuclear ncRNAs and that they might share common RNA substrates, at least in part.

Next, we further examined the target specificities of PARN and TOE1 for these ncRNAs. Interestingly, each class of nuclear

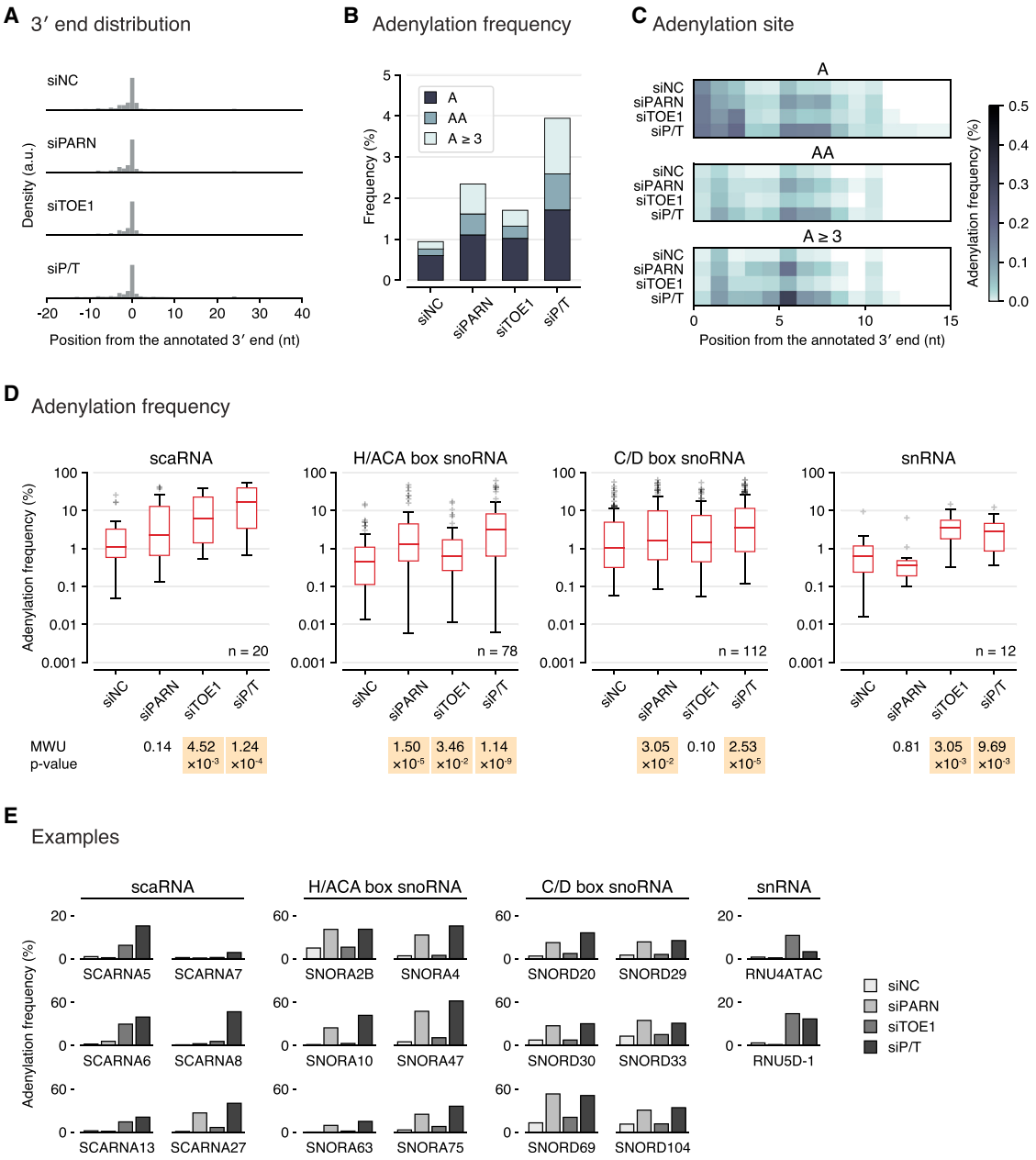

Figure 2. scaRNAs, snoRNAs, and snRNAs Are Major Substrates of PARN and TOE1

(A) 3′ end distribution of scaRNAs, snoRNAs, and snRNAs. Position 0 refers to the 3′ end of transcript described in RefSeq annotation. Negative or positive 3′ end position indicates that the 3′ end of RNA is trimmed or extended, respectively. Density (y. axis) was normalized to the sum of RNA-seq reads corresponding to scaRNAs, snoRNAs, and snRNAs. To filter out 3′ decay products, reads with trimmed end were excluded from the following analyses.

(B) Adenylation frequency of the metagene. A, AA, and A ≥ 3 denote the lengths of 3′ adenosine tail.

(C) Distribution of adenylation sites. Reads were grouped by the length of adenosine tail as in (B).

(D) Boxplots showing the adenylation frequency of each RNA class. Upper and lower bounds of the box indicate the first and third quartiles, respectively, and an internal bar represents the median. Whiskers span between the lowest and highest values within 1.5 times the interquartile range. The statistical significance of differences in adenylation frequency is presented below the boxplots (yellow shaded, $p < 0.05$, one-tailed Mann-Whitney U test).

(E) Adenylation frequency of individual ncRNAs. SCARNA7 is a C/D box RNA while SCARNA8, SCARNA13, and SCARNA27 are H/ACA box RNAs. SCARNA5 and SCARNA6 contain both C/D and H/ACA boxes.

See also Figure S2 and Table S2.

ncRNAs exhibited different sensitivities upon the knockdown of PARN or TOE1 (Figures 2D and 2E). For example, the adenylation frequency of snRNAs increased in TOE1-depleted cells but slightly decreased in PARN-depleted cells, suggesting that TOE1 is the deadenylase for snRNAs. Notably, snoRNAs and scaRNAs, previously identified as PARN substrates, were also affected by TOE1 knockdown. Moreover, the concurrent knockdown of PARN and TOE1 resulted in a greater accumulation of adenylated precursors of scaRNAs and snoRNAs (Figures 2D and 2E). These observations strongly support the functional overlap between PARN and TOE1 for snoRNAs and scaRNAs. Although snoRNAs and scaRNAs are targeted by both enzymes, scaRNAs were more dependent on TOE1 than on PARN, while snoRNAs were more sensitive to PARN knockdown than to TOE1 knockdown. Considering that these enzymes localize to distinct structures in the nucleus, this result suggests that their target specificities might be determined by unique localization pattern of different ncRNA classes.

Also noted is that the adenylation frequency differed substantially among ncRNA classes. When both PARN and TOE1 were depleted, scaRNAs showed the highest frequency of adenylation (median 16.4%), followed by snoRNAs (median 3.4%) and snRNAs (median 2.9%) (Figure 2D). We also found that the distribution of adenylation sites differed among ncRNAs. While adenylation was enriched on 3′-extended precursors of scaRNAs and H/ACA box snoRNAs, this pattern was much less evident for C/D box snoRNAs and snRNAs (Figure S2D). Overall, although both PARN and TOE1 are involved in the 3′ end maturation process of nuclear ncRNAs and can act together in some cases, their action mechanism and functional importance could vary among classes of ncRNAs. The frequency of adenylation on 3′-extended precursors is a good measure of the necessity of each deadenylase for the proper maturation of nuclear ncRNAs (see below).

PARN and TOE1 Protect Maturing scaRNAs from Nuclear RNA Surveillance

In the nucleus, adenylation is utilized to label cryptic and aberrant transcripts and recruits the exosome complex to degrade them (Houseley et al., 2006). Tailing in this quality control process is mediated by the Trf4/5-Air1/2-Mtr4 polyadenylation (TRAMP) complex (LaCava et al., 2005; Vanácová et al., 2005; Wyers et al., 2005). Previous studies revealed that the human TRAMP complex competes with PARN, leading to the destabilization of premature RNAs in the absence of PARN (Boyraz et al., 2016; Moon et al., 2015; Nguyen et al., 2015; Shukla et al., 2016; Tseng et al., 2015). To investigate whether TOE1 also competes with the TRAMP complex, we selected RNAs with significant changes in the 3′ end profile from RNA sequencing (RNA-seq) data (Figure S3A), and we assessed changes in RNA processing and stability by northern blotting (Figure 3A). Even upon the individual knockdown of PARN and TOE1 for a short period (i.e., 2 days), a small fraction of SCARNA8 and SNORA63 was observed in extended forms (Figure 3A, lanes 2 and 3). Moreover, the simultaneous depletion of both enzymes resulted in the further accumulation of longer precursors (lane 4). SCARNA13 also showed a pattern similar to that of SCARNA8, albeit to a lesser extent. Notably, after a prolonged period (4 days), double knockdown led to a strong decrease in mature scaRNA levels and also reduced their extended forms (Figure 3A, lane 8). These data suggest that PARN and TOE1 act redundantly on scaRNAs to remove adenosine tails, which induce the degradation of immature RNAs. qRT-PCR confirmed that SCARNA8 and SCARNA13 were destabilized as the adenylated RNA portion increased, especially upon the co-depletion of PARN and TOE1 (Figures 3C and S3B). This inverse correlation between RNA abundance and adenylation frequency was also found in the RNA-seq analysis (Figure S3C).

To determine whether scaRNA destabilization is dependent on TRAMP activity, we also knocked down TUT3 (PAPD5/TRF4-2), which is one of the main components of the TRAMP complex, in addition to PARN and TOE1. TUT2 (PAPD4/GLD2) and TUT5 (PAPD7/TRF4-1), which are not associated with the TRAMP complex, were depleted in parallel. TUT3 knockdown reversed the accumulation of adenylated processing intermediates and restored the levels of SCARNA8 and SCARNA13 (Figures 3B and 3C), showing that the TRAMP complex is in charge of the adenylation and decay of processing intermediates. However, as PARN and TOE1 are known to favor adenosine the most, adenylation by TUT3 may also be able to enhance deadenylase-mediated trimming. If so, adenylation has a dual role in nuclear RNA biogenesis, and its effect is dependent on the availability of PARN and TOE1. TUT3 knockdown restored scaRNA levels when both PARN and TOE1 were depleted (Figures 3B and 3C), indicating that TUT3 promotes scaRNA decay when PARN and TOE1 levels are low. On the other hand, the single knockdown of TUT3 led to divergent outcomes depending on RNA species (Figures S4A and S4B). This suggests that some nuclear ncRNAs requires adenosine tails to become optimal substrates for PARN and TOE1. Taken together, PARN and TOE1 influence the expression of functional scaRNAs and snoRNAs by competing against adenylation-mediated RNA decay.

Pseudouridylation of snRNA Is Affected by scaRNA Destabilization

scaRNAs localize to Cajal bodies and direct snRNA modification. To address whether the destabilization of scaRNA has a functional consequence in snRNA modification, we examined the pseudouridylation status after PARN/TOE1 double knockdown. For the analysis, we used SCARNA13, which showed a substantial decrease in RNA level (Figures 3C and S3B), and its predicted target site on U5 snRNA (U53) (Lestrade and Weber, 2006; Schattner et al., 2006). To detect pseudouridine residues, total RNAs were subjected to *N*-Cyclohexyl-*N*′-(2-morpholinoethyl)carbodiimide metho-*p*-toluenesulfonate (CMC) modification followed by primer extension for U5 snRNA. Consistent with our prediction, we found that impaired biogenesis of SCARNA13 led to decreased pseudouridylation at the residue U53 of U5 snRNA (Figure 3D). Although the role of pseudouridine is not clear, it has been postulated that the pseudouridine residue influences the RNA secondary structure and RNP assembly (Ge and Yu, 2013). Our findings suggest that a reduction in scaRNA production due to the absence of PARN or TOE1 may have an impact on snRNP assembly and spliceosomal functionality.

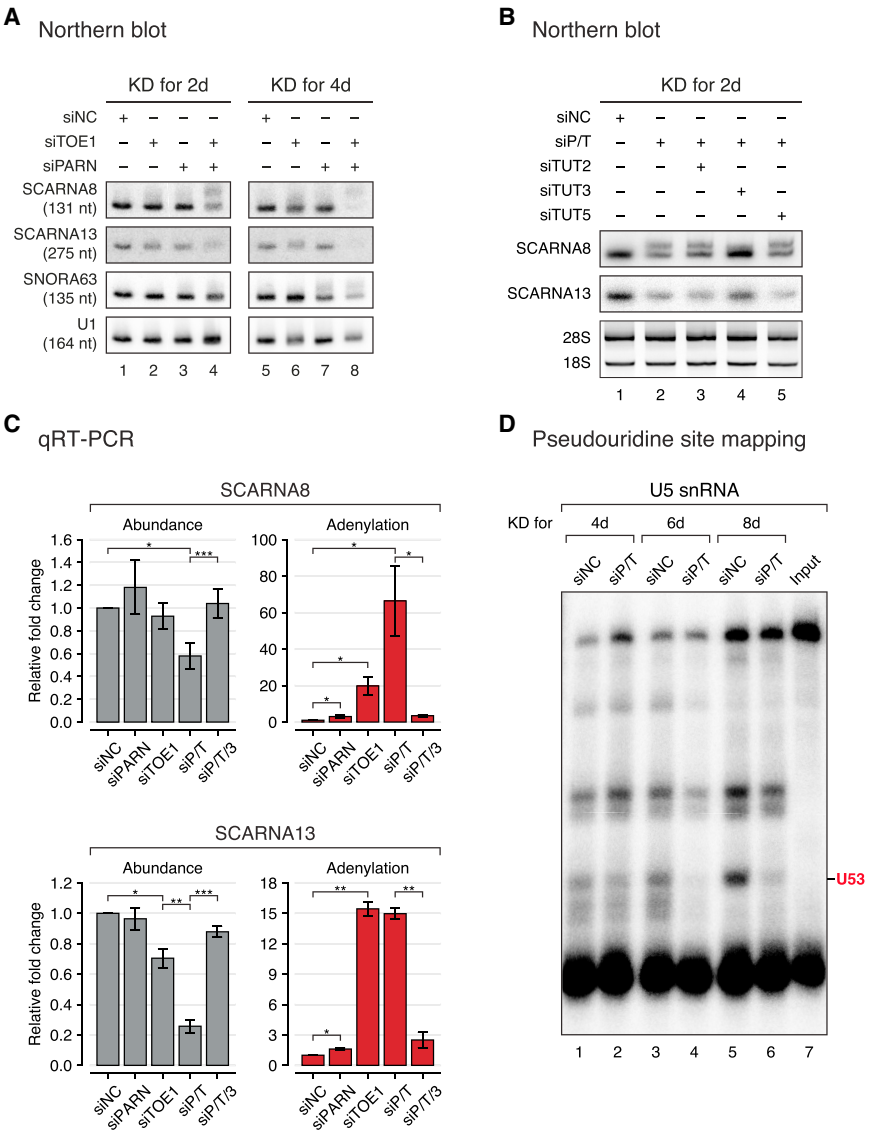

Figure 3. PARN and TOE1 Guard Processing Intermediates of scaRNAs from Adenylation-Dependent RNA Quality Control

(A and B) Northern blot analysis of short ncRNAs using total RNAs prepared from HeLa cells treated with the indicated siRNAs. The lengths of mature transcripts are in parentheses (A). As a loading control, total RNAs (1 μg) were separated on 1% agarose gel and stained with ethidium bromide (B).

(C) qRT-PCR measurements of SCARNA8 and SCARNA13. RNAs were prepared from knockdown and control HeLa cells, and cDNAs were synthesized with gene-specific or oligo(dT) primers. Relative RNA level was measured using gene-specific cDNAs, and adenylation frequency was estimated as the ratio of oligo(dT)-primed cDNAs to gene-specific cDNAs. The measurements were normalized to the *EEF2* mRNA levels measured with corresponding primers, i.e., either oligo(dT) or gene-specific oligonucleotides. siP/T/3 represents PARN/TOE1/TUT3-depleted HeLa cells. Error bars represent SEM (n = 3), and asterisks indicate statistical significance of differences in RNA abundance or adenylation (*$p < 0.05$, **$p < 0.01$, ***$p < 0.001$, one-tailed paired t test).

(D) Pseudouridine residues of U5 snRNA detected by CMC treatment and primer extension following simultaneous PARN and TOE1 knockdown. Since reverse transcription stops a nucleotide prior to CMC adduct, each band represents a putative pseudouridine site. For a negative control, RNAs treated without CMC were loaded on lane 7. The residue U53 of U5 snRNA is a predicted target site of SCARNA13.

See also Figures S3 and S4.

TOE1 Is Involved in the 3′ End Processing of TERC

TERC contains a Cajal body localization signal called the CAB box and 3′ H/ACA box-like domain, which are characteristics of H/ACA box scaRNAs (Jády et al., 2004). The structural similarity between TERC and scaRNAs led us to hypothesize that TOE1 may have a functional role in TERC processing. To validate this, we analyzed RNA-seq reads mapped to TERC, and we found that the proportion of transcripts with adenylation tails increased upon PARN or TOE1 knockdown (Figure 4A). Next, we measured the expression level and adenylation frequency of TERC by qRT-PCR (Figure 4B). In accordance with previous findings (Boyraz et al., 2016; Dhanraj et al., 2015; Moon et al., 2015; Nguyen et al., 2015; Shukla et al., 2016; Tseng et al., 2015), PARN knockdown resulted in an increase in adenylation. Notably, the adenylation frequency also rose slightly in response to TOE1 knockdown, and co-depletion with PARN reinforced this effect. This tendency is analogous to H/ACA box snoRNAs, which have a higher dependency on PARN, and it indicates that TERC is a common target of PARN and TOE1. Of note, TERC level was rescued in TUT3-depleted cells, confirming that TUT3-mediated adenylation leads to TERC degradation (Figures 4B and S4B).

TERC contains the sequence region that forms the base pairing with telomeric repeats and serves as a template for telomere lengthening. To confirm whether TOE1 is also required for telomerase function, we performed a telomeric repeat amplification protocol (TRAP) analysis to measure telomerase activity *in vitro* (Figure 4C). Compared to the control siRNA transfection, individual knockdowns of PARN and TOE1 did not have a notable effect. However, synchronous knockdown of both enzymes vastly reduced telomerase activity. Collectively, not only PARN but also TOE1 plays a pivotal role in TERC biogenesis and function.

DISCUSSION

In this study, we investigated the targetome of two functionally related deadenylases, PARN and TOE1. By analyzing the 3′ ends of mRNAs and short ncRNAs, we showed that both enzymes act on nuclear ncRNAs rather than mRNAs. This is consistent with their localization to nuclear foci and recent

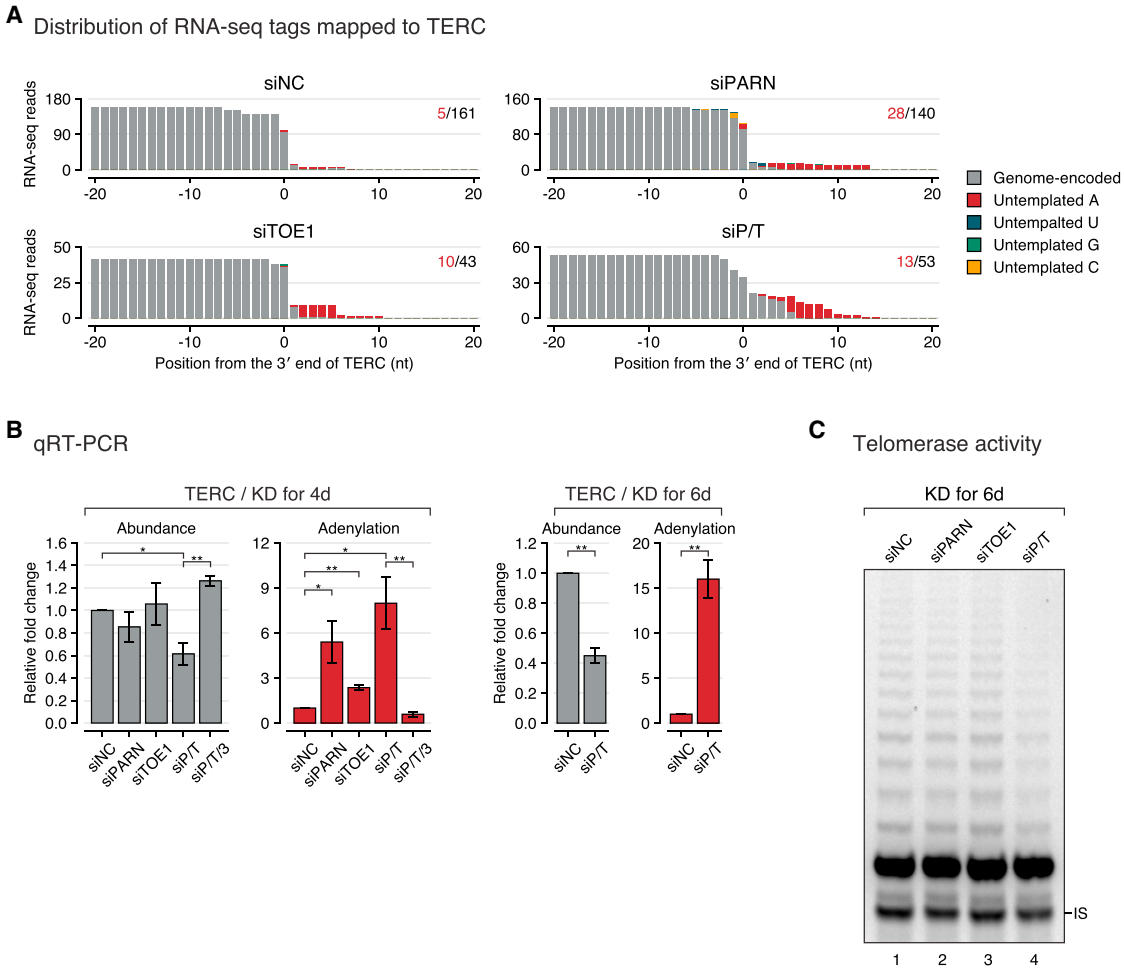

Figure 4. TOE1, as well as PARN, Mediates the 3′ End Processing of Telomerase RNA Component

(A) Distribution of RNA-seq reads corresponding to TERC. The proportion of reads with adenosine tail was shown at the upper right corner of each panel.

(B) qRT-PCR analysis of TERC level and adenylation frequency, as described in Figure 3C. Error bars represent SEM (knockdown for 4 days, n = 4; knockdown for 6 days, n = 3), and asterisks indicate statistical significance of differences in abundance or adenylation of TERC (*p < 0.05, **p < 0.01, one-tailed paired t test).

(C) Telomeric repeat amplification protocol (TRAP) assay for the assessment of telomerase activity in HeLa cells treated with the indicated siRNAs. IS, internal standard.

See also Figure S4.

findings that they function in the biogenesis of various ncRNAs (Berndt et al., 2012; Ishikawa et al., 2017; Montellese et al., 2017; Moon et al., 2015; Nguyen et al., 2015; Shukla and Parker, 2017; Tseng et al., 2015). Nevertheless, we do not exclude the possibility that these enzymes could target mRNAs in the cytoplasm in circumstances that could not be recapitulated in cell culture conditions, such as during oogenesis (Copeland and Wormington, 2001; Kim and Richter, 2006; Körner et al., 1998) or DNA damage (Reinhardt et al., 2010).

This study confirms and expands the model that PARN and TOE1 mediate the 3′ end maturation of short ncRNAs (Figure 5A). These ncRNAs are first transcribed with 3′ trailer sequences and targeted by the nuclear exosome complex (Allmang et al., 1999; Mitchell et al., 2003; van Hoof et al., 2000). The human exosome complex, however, cannot degrade the entire portion and leaves a short tail. These processing intermediates are often adenylated by TUT3, a member of the TRAMP complex. Although adenylation by the TRAMP complex initiates RNA decay in general, PARN and TOE1 compete with the exosome complex and rescue RNAs from the surveillance system. Unlike other conventional deadenylases, this processing also trims the remaining genome-encoded stub. Therefore, we propose that PARN and TOE1 act as trimmers for short nuclear ncRNAs, whose intrinsic specificity to adenosine residues makes them strong safeguards for adenylated intermediates and shields them against the decay process.

Our genome-wide analysis provides a comprehensive view on the targetome of PARN and TOE1 (Figure 5B). In general, target specificities of PARN and TOE1 coincide well with their localization pattern; PARN is localized in the nucleolus and TOE1 is mostly confined to Cajal bodies (Figures 1B and 1C). Although it was reported that PARN also resides in the Cajal bodies (Berndt et al., 2012), we did not detect the protein in the Cajal

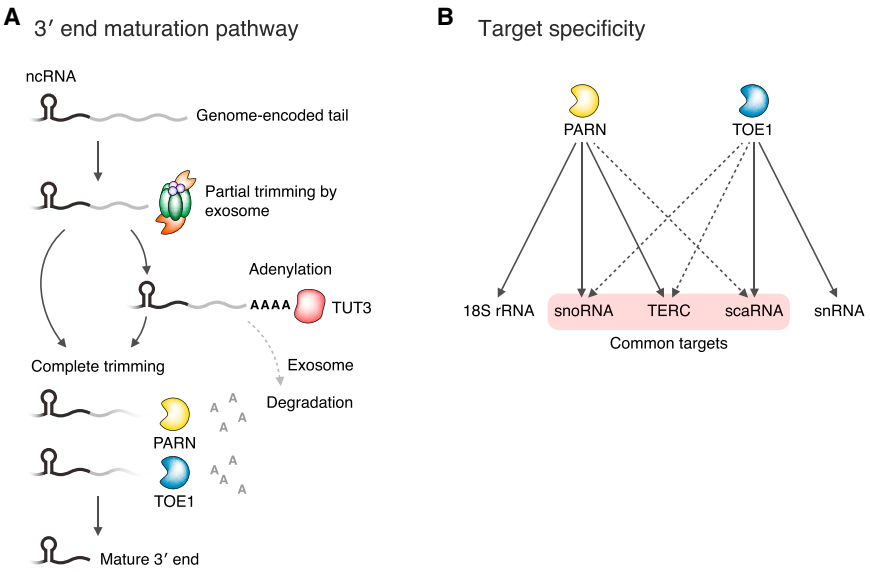

Figure 5. 3′ End Maturation of Nuclear ncRNAs

(A) Schematic illustration of 3′ end maturation pathway.

(B) Target specificity of PARN and TOE1. Each line reflects the degree of precursor RNA accumulation upon deadenylase knockdown. Dashed, moderate; solid, significant.

See also Figure S5.

bodies of HeLa cells (Figure 1B). This is supported by our results showing that snRNAs, which mature in the Cajal body, are solely dependent on TOE1 (Figures 2D and 2E). Moreover, the depletion of PARN delayed the 3′ end processing of 18S rRNA in the nucleolus (Ishikawa et al., 2017; Montellese et al., 2017), whereas TOE1 knockdown did not have any effect on rRNA processing (Figure S5). Thus, we propose that PARN and TOE1 localize to physically distinct environments, and any overlap between their targets could be explained by the length of time that each RNA spends in the two compartments. For example, some snoRNAs initially undergo maturation in the Cajal bodies before they move into the nucleolus (Kiss et al., 2006). Our results support this notion and additionally suggest that the 3′ end trimming of snoRNAs happens predominantly in the nucleolus with little contribution from Cajal bodies. The opposite may be true for scaRNAs, which are more dependent on TOE1 than PARN. Intriguingly, while TERC has been regarded as a kind of scaRNA (Jády et al., 2004), it showed a snoRNA-like pattern in our analysis. This should be validated in the future, once it becomes possible to image maturing ncRNAs at high resolution. We cannot rule out the possibility that other factors, such as interacting proteins and RNA structures, contribute to their specificities.

Finally, our results show that many nuclear ncRNAs (with the exception of snRNAs and 18S rRNA) are redundantly targeted by PARN and TOE1. This explains why the previous study has failed to detect changes in the level or activity of snoRNAs upon PARN knockdown (Berndt et al., 2012). A significant reduction of mature nuclear small RNAs and their functional consequences could be observed only when two proteins of the redundant nuclear deadenylase family were depleted simultaneously (Figures 3C and S3B). Most notably, TERC biogenesis and telomerase activity were strongly reduced only in the double knockdown condition (Figures 4B and 4C). This reveals TOE1 as a contributor to telomerase biogenesis and a potential determinant of telomerase-related pathologies. Further genetic studies are required to unravel the interplay between PARN and TOE1 in human genetic disorders.

EXPERIMENTAL PROCEDURES

Cell Culture

HeLa cells were cultured in DMEM (Welgene) supplemented with 9% fetal bovine serum (Welgene). The human cell line was authenticated using ATCC short tandem repeat profiling service.

siRNA Transfection and RNA Extraction

HeLa cells were transfected with 20 nM siRNAs using Lipofectamine 3000 (Thermo Fisher Scientific). Without specification, genes were depleted for 4 days. Equal amounts of four different siRNAs were used for each knockdown. In combinatorial knockdowns, we mixed multiple siRNA pools to have a final concentration of 20 nM per siRNA pool. As a negative control, a commercial control siRNA (Bioneer, SN-1013) was used. Total RNAs were extracted from siRNA-transfected HeLa cells using TRIzol reagent (Thermo Fisher Scientific), according to the manufacturer's protocol, and treated with DNase I (Takara). We purchased siRNAs against *PARN* and *TOE1* from ON-TARGETplus SMARTpool (Dharmacon), and the sequences of other siRNAs used in this study are listed in Table S3.

Immunocytochemistry

HeLa cells were cultured on a gelatin-coated coverslip. After rinsing with PBS, cells were fixed in PBS-diluted 4% formaldehyde (Thermo Fisher Scientific) for 10 min and permeabilized with 0.1% Triton X-100 for 10 min. The permeabilized HeLa cells were blocked for 1 hr in PBS-T containing 1% or 5% BSA and then probed with a mixture of primary antibodies for 2 hr. After washing three times with PBS-T, cells were probed with the Alexa Fluor-conjugated secondary antibodies (Thermo Fisher Scientific; 1:1,000) and DAPI (Sigma-Aldrich) for 1 hr in the dark. Following washing in PBS-T three times, a coverslip was mounted and sealed. The probed proteins were detected with a fluorescence microscope (Zeiss, LSM 700). The following primary antibodies were used for protein detection: rabbit anti-PARN (Abcam, ab188333; 1:500), rabbit anti-TOE1 (Santa Cruz Biotechnology, sc-98564; 1:50), mouse anti-Nucleolin (Abcam, ab136649; 1:100), and mouse anti-Coilin (Abcam, ab87913; 1:100).

Real-Time qPCR

To measure adenylation frequency, cDNAs were prepared using RevertAid reverse transcriptase (Thermo Fisher Scientific) and gene-specific or oligo(dT) primer. The RNA levels were analyzed by SYBR Green assays (Thermo Fisher Scientific) with StepOnePlus Real-Time PCR system (Thermo Fisher Scientific) and normalized to the level of *EEF2* mRNA. Adenylation frequency was estimated as the ratio between the levels of oligo(dT)-primed cDNAs and gene-specific cDNAs. The primer sequences used for reverse transcription and real-time PCR are listed in Table S3.

mTAIL-Seq

mTAIL-seq libraries were prepared using total RNAs from siRNA-transfected HeLa cells as previously described (Lim et al., 2016). Total RNAs (3 μg) were ligated to the 3′ hairpin adapter using T4 RNA ligase 2, truncated KQ (New England Biolabs). The 3′ adapter-ligated RNAs were partially digested by RNase T1 (Thermo Fisher Scientific) and subject to streptavidin beads (Thermo

Fisher Scientific). The 5′ phosphorylation by T4 PNK (Takara) and endonucleolytic cleavage by APE1 (New England Biolabs) were performed on beads. The eluate was then run on 6% Urea-PAGE gel, and RNAs in the range of 300–750 nt were purified. The extracted RNAs were ligated to 5′ adapter using T4 RNA ligase 1 (New England Biolabs) and copied by SuperScript III reverse transcriptase (Thermo Fisher Scientific) and reverse transcription (RT) primer. cDNAs were amplified by PCR using Phusion High-Fidelity DNA polymerase (Thermo Fisher Scientific), 5′ and 3′ PCR primers. The amplified cDNA library was purified by AMPure XP beads (Beckman Coulter Genomics), and it was sequenced on an Illumina MiSeq platform with 50% of the PhiX control library (Illumina) and 10% of the spike-in mixture. Each spike-in was prepared as in library construction and barcoded for multiplexing (Chang et al., 2014). The sequences of adapters and primers used in library construction are listed in Table S3.

RNA-Seq for Short Non-coding RNAs

For each knockdown, rRNAs were depleted from 5 μg total RNAs using Ribo-Zero H/M/R kit (Illumina). rRNA-depleted RNAs were then ligated to the 3′ adapter with T4 RNA ligase 2, truncated KQ (New England Biolabs). Subsequently, reactants were separated on 6% Urea-PAGE gel to obtain the ligation products in the range of 100–500 nt. The following 5′ adapter ligation, reverse transcription, and cDNA amplification were performed as described in mTAIL-seq library construction. Amplification products were extracted using AMPure XP beads (Beckman Coulter Genomics) and 8% acrylamide gel separation, and the cDNA library was sequenced on an Illumina NextSeq 500 platform. The sequences of adapters and primers are listed in Table S3.

Northern Blot Analysis

Total RNAs were resolved on 10% Urea-PAGE gel and transferred to Hybond-N+ membrane (GE Healthcare). The blotted membrane was UV crosslinked and baked at 80°C for 20 min. The membrane was blocked with 50 μL salmon sperm DNA (Thermo Fisher Scientific) and 5 mL PerfectHyb Plus hybridization buffer (Sigma-Aldrich) for 30 min at 37°C. After prehybridization, 5′ ^{32}P-labeled oligonucleotide probes were added to the solution, and the membrane was incubated for 90 min at 37°C. The membrane was washed twice in wash buffer I (2× saline sodium citrate [SSC] and 0.05% sodium dodecyl sulfate [SDS]) and twice in wash buffer II (0.1× SSC and 0.1% SDS). After brief rinsing in wash buffer II, the membrane was exposed to a phosphor screen and signals were detected by Typhoon FLA 7000 phosphorimager (GE Healthcare).

All oligonucleotide probes were radioisotope labeled using T4 PNK (Takara) and purified by Performa spin columns (EdgeBio) according to the manufacturer's protocol. SCARNA8 or SCARNA13 was detected by using a pool of multiple distinct probes. As a loading control, U1 snRNA detection or ethidium bromide staining after agarose gel separation was used. The sequences of probes are listed in Table S3.

Pseudouridine Site Mapping

Total RNAs (20 μg) were incubated in 30 μL 0.17 M CMC (Sigma-Aldrich) in BEU buffer (50 mM Bicine-NaOH [pH 8.0], 4 mM EDTA, and 7 M Urea) for 30 min at 37°C. For a negative control, 30 μL BEU buffer was used without CMC. RNAs were ethanol precipitated, and the pellet was resuspended in 40 μL 50 mM sodium bicarbonate (pH 10.3). After incubating at 37°C for 3 hr, RNAs were re-precipitated and dissolved in water. Eluted RNAs were reverse transcribed using SuperScript III reverse transcriptase (Thermo Fisher Scientific) and ^{32}P-labeled RT primer. Reaction products were treated with Proteinase K (Sigma-Aldrich) and separated on 15% Urea-PAGE gel. The gel was exposed to a phosphor screen at −80°C, and signals were detected by Typhoon FLA 7000 phosphorimager (GE Healthcare). The primer sequences are listed in Table S3.

Telomerase Activity Assay

TRAP assay was performed with slight modifications from the previous protocol (Mender and Shay, 2015). After siRNA transfection, HeLa cells were lysed in the buffer provided by TeloTAGGG Telomerase PCR ELISA PLUS (Sigma-Aldrich). Next, internal standard (IS) and telomerase substrate with 5′ 6-FAM (FAM-TS) were elongated and amplified in a single reaction that employed cell extract (corresponding to 3 × 10^3 cells), Phusion DNA polymerase (Thermo Fisher Scientific), and 10× TRAP buffer (200 mM Tris-HCl [pH 8.0], 15 mM $MgCl_2$, 630 mM KCl, 0.5% Tween 20, and 10 mM EGTA). Reaction products were separated on 10% PAGE gel and visualized through the fluorescein channel of ChemiDoc XRS+ system (Bio-Rad). The oligonucleotide sequences are listed in Table S3.

Poly(A) Length Measurement

All mTAIL-seq data were processed with Tailseeker 3.1.7 (Chang, 2017) according to the standard workflow of the software (https://zenodo.org/record/887547). Mitochondrial genes were excluded from further analysis. The density of poly(A) length was computed according to the source code of Tailseeker. For gene-level analysis, genes with ≥50 poly(A) tags were used. The geometric mean of poly(A) length was used as a representative value for poly(A) length distribution of each protein-coding gene and referred to as Mean poly(A) length. Poly(A) tag counts of four libraries were quantile normalized to show mRNA level changes between them.

Sequence Processing and Alignment of RNA-Seq Libraries

FASTQ files were first processed using cutadapt 1.11 (Martin, 2011) to remove the 5′ and 3′ adapter sequences (cutadapt -a NNNNTGGAATTCTCGGGTGCCAAGG -A GATCGTCGGACTGTAGAACTCTGAAC -m 20). After trimming, reads were collapsed by FASTX-Toolkit 0.0.13.2 (http://hannonlab.cshl.edu/fastx_toolkit). The reads were then mapped to hg38 genome using STAR 2.5.1 (Dobin et al., 2013) (STAR -alignIntronMin 9999999 -outFilterMultipleNmax 1000). The alignments were annotated by using reduced RefSeq transcript set (Chang et al., 2014) and BEDtools 2.26.0 (Quinlan and Hall, 2010), with minimum 50% overlapping (bedtools intersect -f 0.50).

3′ End Analysis for scaRNAs, snoRNAs, and snRNAs

The 3′ end defined in RefSeq transcriptome is considered as the mature 3′ end and termed position 0. In each read 2 alignment, the 5′ most nucleotide and 5′ soft-clipped sequences were regarded as the 3′ end and untemplated addition, respectively. If a read was mapped to multiple loci, the alignment with the shortest modification and nearest annotation was selected. To exclude 3′ decay intermediates, RNA-seq reads with a trimmed 3′ end (position < 0) were disregarded. For metagene analysis, modification frequency was computed by the proportion of reads with corresponding untemplated addition. Using genes with ≥100 reads (with position ≥ 0) in all libraries, adenylation frequency of each RNA was calculated as the percentage of reads with 3′ adenylation (pseudocount = 1). For quantitative comparison, quantile normalization was applied to all nuclear ncRNAs (scaRNAs, snoRNAs, and snRNAs) detected in the RNA-seq.

Quantification and Statistical Analysis

All statistical analyses were performed using R language and SciPy Python module. Statistical parameters and statistical significance are reported in the figure legends; "n" represents the number of genes used in high-throughput sequencing analyses or the experimental replication of qRT-PCR. Data are judged to be statistically significant when $p < 0.01$ by two-tailed Mann-Whitney U test or $p < 0.05$ by one-tailed Mann-Whitney U test and one-tailed paired t test.

DATA AND SOFTWARE AVAILABILITY

The accession number for the RNA-seq data reported in this paper is GEO: GSE111511. The raw data files for the mTAIL-seq have been uploaded to Zenodo and are available at https://doi.org/10.5281/zenodo.1066619. Original imaging data have been deposited to Mendeley Data and are available at https://doi.org/10.17632/vfm55nv4nw.1.

SUPPLEMENTAL INFORMATION

Supplemental Information includes Supplemental Experimental Procedures, five figures, and three tables and can be found with this article online at https://doi.org/10.1016/j.celrep.2018.03.089.

ACKNOWLEDGMENTS

We thank Mihye Lee, Sungyul Lee, Young-suk Lee, Baekgyu Kim, Hyeshik Chang, and other members of our laboratory for discussion and technical help. This work was supported by IBS-R008-D1 from the Institute for Basic Science from the Ministry of Science, ICT and Future Planning of Korea (A.S., J.-E.P., and V.N.K.) and by the BK21 Research Fellowships from the Ministry of Education of Korea (A.S.).

AUTHOR CONTRIBUTIONS

A.S., J.-E.P., and V.N.K. designed experiments. J.-E.P. and A.S. performed mTAIL-seq and RNA-seq, respectively. A.S. and J.-E.P. did biochemical experiments. A.S. carried out computational analyses. A.S., J.-E.P., and V.N.K. wrote the manuscript.

DECLARATION OF INTERESTS

The authors declare no competing interests.

Received: December 2, 2017
Revised: December 27, 2017
Accepted: March 20, 2018
Published: April 17, 2018

REFERENCES

Allmang, C., Kufel, J., Chanfreau, G., Mitchell, P., Petfalski, E., and Tollervey, D. (1999). Functions of the exosome in rRNA, snoRNA and snRNA synthesis. EMBO J. *18*, 5399–5410.

Berndt, H., Harnisch, C., Rammelt, C., Stöhr, N., Zirkel, A., Dohm, J.C., Himmelbauer, H., Tavanez, J.P., Hüttelmaier, S., and Wahle, E. (2012). Maturation of mammalian H/ACA box snoRNAs: PAPD5-dependent adenylation and PARN-dependent trimming. RNA *18*, 958–972.

Boyraz, B., Moon, D.H., Segal, M., Muosieyiri, M.Z., Aykanat, A., Tai, A.K., Cahan, P., and Agarwal, S. (2016). Posttranscriptional manipulation of TERC reverses molecular hallmarks of telomere disease. J. Clin. Invest. *126*, 3377–3382.

Burris, A.M., Ballew, B.J., Kentosh, J.B., Turner, C.E., Norton, S.A., NCI DCEG Cancer Genomics Research Laboratory; NCI DCEG Cancer Sequencing Working Group; Giri, N., Alter, B.P., Nellan, A., et al. (2016). Hoyeraal-Hreidarsson Syndrome due to PARN Mutations: Fourteen Years of Follow-Up. Pediatr. Neurol. *56*, 62–68.e1.

Cevher, M.A., Zhang, X., Fernandez, S., Kim, S., Baquero, J., Nilsson, P., Lee, S., Virtanen, A., and Kleiman, F.E. (2010). Nuclear deadenylation/polyadenylation factors regulate 3′ processing in response to DNA damage. EMBO J. *29*, 1674–1687.

Chang, H. (2017). Tailseeker 3.1.7: the pipeline for high-throughput RNA poly(A) length and 3′ end modification measurement. https://zenodo.org/record/887547#.Wr5KCi7waUk.

Chang, H., Lim, J., Ha, M., and Kim, V.N. (2014). TAIL-seq: genome-wide determination of poly(A) tail length and 3′ end modifications. Mol. Cell *53*, 1044–1052.

Copeland, P.R., and Wormington, M. (2001). The mechanism and regulation of deadenylation: identification and characterization of Xenopus PARN. RNA *7*, 875–886.

Devany, E., Zhang, X., Park, J.Y., Tian, B., and Kleiman, F.E. (2013). Positive and negative feedback loops in the p53 and mRNA 3′ processing pathways. Proc. Natl. Acad. Sci. USA *110*, 3351–3356.

Dhanraj, S., Gunja, S.M., Deveau, A.P., Nissbeck, M., Boonyawat, B., Coombs, A.J., Renieri, A., Mucciolo, M., Marozza, A., Buoni, S., et al. (2015). Bone marrow failure and developmental delay caused by mutations in poly(A)-specific ribonuclease (PARN). J. Med. Genet. *52*, 738–748.

Dobin, A., Davis, C.A., Schlesinger, F., Drenkow, J., Zaleski, C., Jha, S., Batut, P., Chaisson, M., and Gingeras, T.R. (2013). STAR: ultrafast universal RNA-seq aligner. Bioinformatics *29*, 15–21.

Dreyfus, M., and Régnier, P. (2002). The poly(A) tail of mRNAs: bodyguard in eukaryotes, scavenger in bacteria. Cell *111*, 611–613.

Fong, K.W., Li, Y., Wang, W., Ma, W., Li, K., Qi, R.Z., Liu, D., Songyang, Z., and Chen, J. (2013). Whole-genome screening identifies proteins localized to distinct nuclear bodies. J. Cell Biol. *203*, 149–164.

Garneau, N.L., Wilusz, J., and Wilusz, C.J. (2007). The highways and byways of mRNA decay. Nat. Rev. Mol. Cell Biol. *8*, 113–126.

Ge, J., and Yu, Y.T. (2013). RNA pseudouridylation: new insights into an old modification. Trends Biochem. Sci. *38*, 210–218.

Gherzi, R., Lee, K.Y., Briata, P., Wegmüller, D., Moroni, C., Karin, M., and Chen, C.Y. (2004). A KH domain RNA binding protein, KSRP, promotes ARE-directed mRNA turnover by recruiting the degradation machinery. Mol. Cell *14*, 571–583.

Goldstrohm, A.C., and Wickens, M. (2008). Multifunctional deadenylase complexes diversify mRNA control. Nat. Rev. Mol. Cell Biol. *9*, 337–344.

Houseley, J., LaCava, J., and Tollervey, D. (2006). RNA-quality control by the exosome. Nat. Rev. Mol. Cell Biol. *7*, 529–539.

Ishikawa, H., Yoshikawa, H., Izumikawa, K., Miura, Y., Taoka, M., Nobe, Y., Yamauchi, Y., Nakayama, H., Simpson, R.J., Isobe, T., and Takahashi, N. (2017). Poly(A)-specific ribonuclease regulates the processing of small-subunit rRNAs in human cells. Nucleic Acids Res. *45*, 3437–3447.

Jády, B.E., Bertrand, E., and Kiss, T. (2004). Human telomerase RNA and box H/ACA scaRNAs share a common Cajal body-specific localization signal. J. Cell Biol. *164*, 647–652.

Kim, J.H., and Richter, J.D. (2006). Opposing polymerase-deadenylase activities regulate cytoplasmic polyadenylation. Mol. Cell *24*, 173–183.

Kiss, T., Fayet, E., Jády, B.E., Richard, P., and Weber, M. (2006). Biogenesis and intranuclear trafficking of human box C/D and H/ACA RNPs. Cold Spring Harb. Symp. Quant. Biol. *71*, 407–417.

Körner, C.G., Wormington, M., Muckenthaler, M., Schneider, S., Dehlin, E., and Wahle, E. (1998). The deadenylating nuclease (DAN) is involved in poly(A) tail removal during the meiotic maturation of Xenopus oocytes. EMBO J. *17*, 5427–5437.

Kropski, J.A., Reiss, S., Markin, C., Brown, K.K., Schwartz, D.A., Schwarz, M.I., Loyd, J.E., Phillips, J.A., 3rd, Blackwell, T.S., and Cogan, J.D. (2017). Rare Genetic Variants in PARN Are Associated with Pulmonary Fibrosis in Families. Am. J. Respir. Crit. Care Med. *196*, 1481–1484.

LaCava, J., Houseley, J., Saveanu, C., Petfalski, E., Thompson, E., Jacquier, A., and Tollervey, D. (2005). RNA degradation by the exosome is promoted by a nuclear polyadenylation complex. Cell *121*, 713–724.

Lai, W.S., Kennington, E.A., and Blackshear, P.J. (2003). Tristetraprolin and its family members can promote the cell-free deadenylation of AU-rich element-containing mRNAs by poly(A) ribonuclease. Mol. Cell. Biol. *23*, 3798–3812.

Lardelli, R.M., Schaffer, A.E., Eggens, V.R., Zaki, M.S., Grainger, S., Sathe, S., Van Nostrand, E.L., Schlachetzki, Z., Rosti, B., Akizu, N., et al. (2017). Biallelic mutations in the 3′ exonuclease TOE1 cause pontocerebellar hypoplasia and uncover a role in snRNA processing. Nat. Genet. *49*, 457–464.

Lee, J.E., Lee, J.Y., Trembly, J., Wilusz, J., Tian, B., and Wilusz, C.J. (2012). The PARN deadenylase targets a discrete set of mRNAs for decay and regulates cell motility in mouse myoblasts. PLoS Genet. *8*, e1002901.

Lejeune, F., Li, X., and Maquat, L.E. (2003). Nonsense-mediated mRNA decay in mammalian cells involves decapping, deadenylating, and exonucleolytic activities. Mol. Cell *12*, 675–687.

Lestrade, L., and Weber, M.J. (2006). snoRNA-LBME-db, a comprehensive database of human H/ACA and C/D box snoRNAs. Nucleic Acids Res. *34*, D158–D162.

Lim, J., Lee, M., Son, A., Chang, H., and Kim, V.N. (2016). mTAIL-seq reveals dynamic poly(A) tail regulation in oocyte-to-embryo development. Genes Dev. *30*, 1671–1682.

Lin, W.J., Duffy, A., and Chen, C.Y. (2007). Localization of AU-rich element-containing mRNA in cytoplasmic granules containing exosome subunits. J. Biol. Chem. *282*, 19958–19968.

Mao, Y.S., Zhang, B., and Spector, D.L. (2011). Biogenesis and function of nuclear bodies. Trends Genet. *27*, 295–306.

Martin, M. (2011). Cutadapt removes adapter sequences from high-throughput sequencing reads. EMBnet.journal *17*, 10–12.

Matera, A.G., Terns, R.M., and Terns, M.P. (2007). Non-coding RNAs: lessons from the small nuclear and small nucleolar RNAs. Nat. Rev. Mol. Cell Biol. *8*, 209–220.

Mender, I., and Shay, J.W. (2015). Telomerase Repeated Amplification Protocol (TRAP). Bio Protoc. *5*, e1657.

Miller, T.E., and Gomez-Cambronero, J. (2017). A feedback mechanism between PLD and deadenylase PARN for the shortening of eukaryotic poly(A) mRNA tails that is deregulated in cancer cells. Biol. Open *6*, 176–186.

Mitchell, P., Petfalski, E., Houalla, R., Podtelejnikov, A., Mann, M., and Tollervey, D. (2003). Rrp47p is an exosome-associated protein required for the 3′ processing of stable RNAs. Mol. Cell. Biol. *23*, 6982–6992.

Montellese, C., Montel-Lehry, N., Henras, A.K., Kutay, U., Gleizes, P.E., and O'Donohue, M.F. (2017). Poly(A)-specific ribonuclease is a nuclear ribosome biogenesis factor involved in human 18S rRNA maturation. Nucleic Acids Res. *45*, 6822–6836.

Moon, D.H., Segal, M., Boyraz, B., Guinan, E., Hofmann, I., Cahan, P., Tai, A.K., and Agarwal, S. (2015). Poly(A)-specific ribonuclease (PARN) mediates 3′-end maturation of the telomerase RNA component. Nat. Genet. *47*, 1482–1488.

Moraes, K.C., Wilusz, C.J., and Wilusz, J. (2006). CUG-BP binds to RNA substrates and recruits PARN deadenylase. RNA *12*, 1084–1091.

Nguyen, D., Grenier St-Sauveur, V., Bergeron, D., Dupuis-Sandoval, F., Scott, M.S., and Bachand, F. (2015). A Polyadenylation-Dependent 3′ End Maturation Pathway Is Required for the Synthesis of the Human Telomerase RNA. Cell Rep. *13*, 2244–2257.

Petrovski, S., Todd, J.L., Durheim, M.T., Wang, Q., Chien, J.W., Kelly, F.L., Frankel, C., Mebane, C.M., Ren, Z., Bridgers, J., et al. (2017). An Exome Sequencing Study to Assess the Role of Rare Genetic Variation in Pulmonary Fibrosis. Am. J. Respir. Crit. Care Med. *196*, 82–93.

Quinlan, A.R., and Hall, I.M. (2010). BEDTools: a flexible suite of utilities for comparing genomic features. Bioinformatics *26*, 841–842.

Reinhardt, H.C., Hasskamp, P., Schmedding, I., Morandell, S., van Vugt, M.A., Wang, X., Linding, R., Ong, S.E., Weaver, D., Carr, S.A., and Yaffe, M.B. (2010). DNA damage activates a spatially distinct late cytoplasmic cell-cycle checkpoint network controlled by MK2-mediated RNA stabilization. Mol. Cell *40*, 34–49.

Schattner, P., Barberan-Soler, S., and Lowe, T.M. (2006). A computational screen for mammalian pseudouridylation guide H/ACA RNAs. RNA *12*, 15–25.

Schmidt, J.C., and Cech, T.R. (2015). Human telomerase: biogenesis, trafficking, recruitment, and activation. Genes Dev. *29*, 1095–1105.

Shukla, S., and Parker, R. (2017). PARN Modulates Y RNA Stability and Its 3′-End Formation. Mol. Cell. Biol. *37*, e00264-17.

Shukla, S., Schmidt, J.C., Goldfarb, K.C., Cech, T.R., and Parker, R. (2016). Inhibition of telomerase RNA decay rescues telomerase deficiency caused by dyskerin or PARN defects. Nat. Struct. Mol. Biol. *23*, 286–292.

Stuart, B.D., Choi, J., Zaidi, S., Xing, C., Holohan, B., Chen, R., Choi, M., Dharwadkar, P., Torres, F., Girod, C.E., et al. (2015). Exome sequencing links mutations in PARN and RTEL1 with familial pulmonary fibrosis and telomere shortening. Nat. Genet. *47*, 512–517.

Tseng, C.K., Wang, H.F., Burns, A.M., Schroeder, M.R., Gaspari, M., and Baumann, P. (2015). Human Telomerase RNA Processing and Quality Control. Cell Rep. *13*, 2232–2243.

Tummala, H., Walne, A., Collopy, L., Cardoso, S., de la Fuente, J., Lawson, S., Powell, J., Cooper, N., Foster, A., Mohammed, S., et al. (2015). Poly(A)-specific ribonuclease deficiency impacts telomere biology and causes dyskeratosis congenita. J. Clin. Invest. *125*, 2151–2160.

Udagawa, T., Swanger, S.A., Takeuchi, K., Kim, J.H., Nalavadi, V., Shin, J., Lorenz, L.J., Zukin, R.S., Bassell, G.J., and Richter, J.D. (2012). Bidirectional control of mRNA translation and synaptic plasticity by the cytoplasmic polyadenylation complex. Mol. Cell *47*, 253–266.

van Hoof, A., Lennertz, P., and Parker, R. (2000). Yeast exosome mutants accumulate 3′-extended polyadenylated forms of U4 small nuclear RNA and small nucleolar RNAs. Mol. Cell. Biol. *20*, 441–452.

Vanácová, S., Wolf, J., Martin, G., Blank, D., Dettwiler, S., Friedlein, A., Langen, H., Keith, G., and Keller, W. (2005). A new yeast poly(A) polymerase complex involved in RNA quality control. PLoS Biol. *3*, e189.

Virtanen, A., Henriksson, N., Nilsson, P., and Nissbeck, M. (2013). Poly(A)-specific ribonuclease (PARN): an allosterically regulated, processive and mRNA cap-interacting deadenylase. Crit. Rev. Biochem. Mol. Biol. *48*, 192–209.

Wagner, E., Clement, S.L., and Lykke-Andersen, J. (2007). An unconventional human Ccr4-Caf1 deadenylase complex in nuclear cajal bodies. Mol. Cell. Biol. *27*, 1686–1695.

Wyers, F., Rougemaille, M., Badis, G., Rousselle, J.C., Dufour, M.E., Boulay, J., Régnault, B., Devaux, F., Namane, A., Séraphin, B., et al. (2005). Cryptic pol II transcripts are degraded by a nuclear quality control pathway involving a new poly(A) polymerase. Cell *121*, 725–737.

Yamashita, A., Chang, T.C., Yamashita, Y., Zhu, W., Zhong, Z., Chen, C.Y., and Shyu, A.B. (2005). Concerted action of poly(A) nucleases and decapping enzyme in mammalian mRNA turnover. Nat. Struct. Mol. Biol. *12*, 1054–1063.

Yoda, M., Cifuentes, D., Izumi, N., Sakaguchi, Y., Suzuki, T., Giraldez, A.J., and Tomari, Y. (2013). Poly(A)-specific ribonuclease mediates 3′-end trimming of Argonaute2-cleaved precursor microRNAs. Cell Rep. *5*, 715–726.

Zhang, L.N., and Yan, Y.B. (2015). Depletion of poly(A)-specific ribonuclease (PARN) inhibits proliferation of human gastric cancer cells by blocking cell cycle progression. Biochim. Biophys. Acta *1853*, 522–534.

Zhang, X., Devany, E., Murphy, M.R., Glazman, G., Persaud, M., and Kleiman, F.E. (2015). PARN deadenylase is involved in miRNA-dependent degradation of TP53 mRNA in mammalian cells. Nucleic Acids Res. *43*, 10925–10938.

Zhu, Y., Chen, G., Lv, F., Wang, X., Ji, X., Xu, Y., Sun, J., Wu, L., Zheng, Y.T., and Gao, G. (2011). Zinc-finger antiviral protein inhibits HIV-1 infection by selectively targeting multiply spliced viral mRNAs for degradation. Proc. Natl. Acad. Sci. USA *108*, 15834–15839.